electronics

Article

Research on the Evaluation and Prediction of V2I Channel Quality Levels in Urban Environments

Shengli Pang, Zekang Li, Ziru Yao, Honggang Wang, Weichen Long and Ruoyu Pan *

School of Communications and Information Engineering, Xi'an University of Posts and Telecommunications, Xi'an 710121, China; pangshengli@xupt.edu.cn (S.P.); lizekang@stu.xupt.edu.cn (Z.L.); yaoziru@stu.xupt.edu.cn (Z.Y.); wanghonggang@xupt.edu.cn (H.W.); longweichen@stu.xupt.edu.cn (W.L.)
* Correspondence: panruoyu@xupt.edu.cn

Abstract: The present manuscript introduces a method for evaluating and forecasting the quality of vehicle-to-infrastructure (V2I) communication channels in urban settings. This method precisely classifies and predicts channel quality levels in V2I scenarios based on long-range (LoRa) technology. This approach aims to accurately classify and predict channel quality levels in V2I scenarios. The concept of channel quality scoring was first introduced, offering a more precise description of channel quality compared to traditional packet reception rate (PRR) assessments. In the channel quality assessment model based on the gated recurrent unit (GRU) algorithm, the current channel quality score of the vehicular terminal and the spatial channel parameters (SCP) of its location are utilized as inputs to achieve the classification of channel quality levels with an accuracy of 97.5%. Regarding prediction, the focus lies in forecasting the channel quality score, combined with the calculation of SCP for the vehicle's following temporal location, thereby achieving predictions of channel quality levels from spatial and temporal perspectives. The prediction model employs the Variational Mode Decomposition-Backoff-Bidirectional Long Short-Term Memory (VMD-BO-BiLSTM) algorithm, which, while maintaining an acceptable training time, exhibits higher accuracy than other prediction algorithms, with an R^2 value reaching 0.9945. This model contributes to assessing and predicting channel quality in V2I scenarios and holds significant implications for subsequent channel resource allocation.

Keywords: channel quality levels; V2I; LoRa; GRU; VMD-BO-BiLSTM

Citation: Pang, S.; Li, Z.; Yao, Z.; Wang, H.; Long, W.; Pan, R. Research on the Evaluation and Prediction of V2I Channel Quality Levels in Urban Environments. *Electronics* **2024**, *13*, 911. https://doi.org/10.3390/electronics13050911

Academic Editors: Daniel Gutiérrez Reina and Erich Leitgeb

Received: 10 January 2024
Revised: 20 February 2024
Accepted: 25 February 2024
Published: 27 February 2024

1. Introduction

With the rapid advancement of electronic information technology, vehicle-to-everything (V2X) technology has transformed automobiles from individual units into interconnected and intelligent entities [1,2]. V2X technology facilitates the interconnection of vehicles with the environment, encompassing vehicle-to-vehicle (V2V) and vehicle-to-infrastructure (V2I) communications [3]. V2V communication involves vehicle interactions, while V2I encompasses communications between vehicles and roadside infrastructure (such as traffic lights, control towers, or other facilities). Leveraging V2X technology enables collision avoidance, reduced travel time, and autonomous driving, meeting the requirements for future intelligent transportation, globalized traffic management, and ubiquitous information services [4]. As the number of vehicles rapidly escalates, V2X communication critically requires a new paradigm to satisfy its increasing connectivity demands, primarily addressing support for numerous devices, low deployment costs, extended coverage, low device expenses, and prolonged battery life.

The Low-Power Wide Area Network (LPWAN) boasts long-range connectivity, low power consumption, cost-effectiveness, and extensive network capacity. Within the realm of LPWAN, LoRa technology primarily targets the Internet of Things (IoT) applications. Its exceptionally high sensitivity ensures the reliability of network connections, while the deficient power consumption allows for prolonged terminal operation post-deployment [5]. LoRa employs linear frequency modulation spread spectrum modulation, which enhances communication distance while maintaining the low-power characteristics similar to frequency-shift keying (FSK) modulation. The use of spreading factors improves network efficiency and eliminates interference. Building upon this foundation, concentrators/gateways are developed to receive and process data from multiple terminals concurrently, significantly expanding system capacity. As an LPWAN wireless technology operating in an unlicensed spectrum, LoRa demonstrates relatively faster progress in technology development and commercialization compared to other wireless technologies such as Sigfox and NWave, making it more suitable for application in the context of vehicular networking scenarios [6].

Some of the primary challenges in V2X communication include time-criticality, latency tolerance, security, and privacy [7–9]. Furthermore, channel quality is susceptible to multipath effects, loss attenuation, and adjacent channel interference in communication. These influences may lead to the loss of some business data, resulting in data packet retransmission or terminal re-entry into the network. Low channel quality not only increases communication delay but also undermines network stability. Effective channel resource allocation can reduce retransmissions, save system power, increase network capacity, and ensure network robustness. Channel resource allocation relies on channel quality assessment. A reliable channel quality assessment method can make channel resource allocation more effective. This paper investigates the channel quality assessment of LoRa networks in V2I scenarios. In contrast to the need for more existing research in evaluating channel quality, this study introduces a novel channel quality assessment system (channel quality scoring) to provide a more detailed description of the variability of channel quality. Building upon this framework, the assessment of channel quality levels in various operational scenarios is achieved by integrating vehicle position information and classification algorithms.

The remaining sections of this paper are organized as follows: Section 2 presents related work. Section 3 introduces the fundamental principles of channel quality scoring models, channel quality assessment, and prediction. Section 4 provides a detailed description of establishing the channel quality scoring model and the channel quality assessment and prediction model. Section 5 validates the models through specific tests. Finally, Section 6 outlines the conclusions of this paper and suggests avenues for future expansion.

2. Relevant Studies

Currently, there is a growing body of research on applying LoRa networks in the context of vehicular communication. In [10], the authors compared the simulation and empirical data of LoRa network communication metrics in V2X scenarios. The experimental results demonstrated that the observed packet delivery ratio (PDR), packet reception time (PIR), and received signal strength indicator (RSSI) were consistent with the simulation results (excluding complex interference environments). In [11], simulation using the ns-3 module confirmed that the LoRa-based IoT network achieved a packet success reception rate of over 95% for multiple end devices in typical urban scenarios. Furthermore, [6] investigated the Doppler effect caused by rapid vehicular movement in LoRa networks and proposed altering communication parameters to mitigate the fast fading induced by the Doppler effect. Moreover, [12] presented a V2X communication architecture employing LoRa wireless technology. This architecture enhances communication reliability by enabling direct V2V and V2X communication, further improving communication latency.

In the context of vehicular communication, the assessment of channel quality is crucial for various aspects, such as network resource scheduling management [13], access schemes [14], and route selection [15]. Addressing the imbalance in wireless channel samples, [16] proposes a channel quality estimation method that combines the K-means Synthetic Minority Over-sampling Technique (K-means SMOTE) and weighted random forests. This method utilizes the mean, variance, and asymmetry index of physical layer parameters as channel quality indicators. To overcome the limitations of relying solely on physical layer parameters to characterize channel quality clearly, [17] introduces a novel method, SeqLQE, which utilizes system metrics—such as radio link establishment time and received packet count—rather than physical layer measurements to predict channel quality. By designing and collecting runtime measurements during network operation and using a Seq2Seq learning model to capture the correlation structure between channel quality and system metrics, this approach aims to provide a more comprehensive representation of channel quality. Furthermore, [18] proposes a deep-forest-based link quality estimation model, starting from data preprocessing. An improved K-center points algorithm based on stepwise increment and optimized centroids (INCK) is utilized in partitioning channel quality levels to address the issue of noisy samples becoming cluster centroids. By incorporating hierarchical sampling to alter the imbalanced distribution of channel quality samples, the feature extraction performance of the deep forest model is enhanced. Current research directions in channel quality evaluation and prediction mainly focus on representing channel quality using different parameters and selecting suitable prediction algorithms. However, there is limited research on the sensitivity of business requirements to channel quality. This study investigates channel quality assessment and prediction by integrating business characteristics based on existing research. Given the significant advantages demonstrated by specific machine learning algorithms in predicting weather, traffic flow, disease development, and object recognition and classification problems [19–22], these algorithms are increasingly being applied to address communication issues [23]. This study will utilize machine learning algorithms to investigate the assessment and prediction of channel quality levels.

3. Theoretical Basis of Channel Quality Assessment and Prediction Model

3.1. Characteristics of Channel in Urban Mobility Scenarios

The term "path loss" (PL) refers to the average fading of the signal between the transmitter and the receiver. It is typically logarithmically related to the frequency and distance and can be expressed as:

$$\mathrm{PL}(d,f) = 32.45 + 20\lg(d) + 20\lg(f) + S_\sigma \tag{1}$$

Here, $\mathrm{PL}_0 = 32.45 + 20\lg(d) + 20\lg(f)$ represents the free space path loss, indicating the signal attenuation when there is no obstruction between the transmitter and receiver. Where f is the signal frequency in MHz, and d is the distance between the transmitter and receiver in kilometers. S_σ represents the shadowing loss, which accounts for additional propagation environment-induced losses beyond the distance factor, such as building density and height. In the context of vehicular networks, the transmission path between the receiver and the transmitter undergoes continuous changes with the movement of vehicles. This paper will introduce the study of SCP to analyze the variation in channel environment between the vehicular terminal and the gateway during vehicular movement.

3.1.1. The Phenomenon of Multipath Interference

The V2I communication environment is complex and diverse, with signals potentially undergoing reflection, scattering, and diffraction to reach the receiver through multiple transmission paths. The superposition and coherent interference of electromagnetic waves from different paths at the receiving end can lead to changes in the amplitude and phase of the received signal, known as multipath fading. Based on whether the electromagnetic waves undergo scattering during propagation, all rays reaching the receiver are classified into Line of Sight (LoS) and Non-Line of Sight (NLoS) rays. When a stable main signal exists in the communication channel environment, its small-scale fading envelope follows a Rice distribution, and the Rice factor K accurately describes this distribution. The Rice factor K directly determines the power ratio between the LOS component and the NLOS component, making it a key parameter for characterizing channel quality.

3.1.2. Vehicular Traffic Density

Vehicular Traffic Density (VTD) is a unique concept in vehicular communication employed to characterize the density of vehicles on a roadway. A higher VTD implies lower spatiotemporal correlation properties, a more concentrated distribution of scatterers, and increased spatiotemporal correlation.

3.2. Basic Theory of Channel Quality Scoring

3.2.1. Parameters for Evaluating Channel Quality

The assessment model of channel quality in V2I scenarios should objectively, accurately, and comprehensively reflect the quality of the channel for vehicles in motion. More than merely relying on the simple PRR is required for a comprehensive representation of channel quality. PRR can only indicate the quality of the channel within a specific period, and the channel is susceptible to interference due to its open nature. The variation in channel quality is a dynamic process and can be represented based on the reception conditions of multiple window messages. This dynamic process of representation can be divided into the intensity of short-term channel quality changes and the long-term trend of changes. The long-term trend of channel quality can be represented through PRR. In this paper, the short-term changes in channel quality are characterized through the statistical characteristics of signal strength and signal-to-noise ratio of uplink data from vehicular terminals within a specific interval.

r^i_{RSSI} and r^i_{SNR} represent the short-term change increments of the signal-to-noise ratio and signal strength at time i as the difference between the current value and the average value within the statistical window N, as shown in Equations (2) and (3). Here, SNR_i and $RSSI_i$, respectively, denote the signal-to-noise ratio and signal strength at time i. $\overline{SNR_N}$ and $\overline{RSSI_N}$ represent the average values of the most recent N data frames for the signal-to-noise ratio and signal strength. The stability of channel quality within the time window N is represented by the variance of signal strength σ^2_{RSSI} and the variance of signal-to-noise ratio σ^2_{SNR}, as shown in Equation (4).

$$\overline{SNR_N} = \frac{\sum\limits_{j=i-N+1}^{i} SNR_j}{N},\ \overline{RSSI_N} = \frac{\sum\limits_{j=i-N+1}^{i} RSSI_j}{N} \tag{2}$$

$$r^i_{SNR} = SNR_i - \overline{SNR_N},\ r^i_{RSSI} = RSSI_i - \overline{RSSI_N} \tag{3}$$

$$\sigma^2_{RSSI} = \frac{\sum\limits_{j=i-N+1}^{i} (\overline{RSSI_N} - RSSI_j)^2}{N},\ \sigma^2_{SNR} = \frac{\sum\limits_{j=i-N+1}^{i} (\overline{SNR_N} - SNR_i)^2}{N} \tag{4}$$

The evaluation of channel quality includes measuring the parameters that define channel quality and the composition of the weights associated with each parameter. The weights for each parameter are computed through a method of combined weighting. The subjective weights are initially calculated using the fuzzy analytic hierarchy process, while the objective weights are determined using the entropy weight method. Subsequently, the weights for each parameter are obtained through a combined weighting process employing the critic algorithm. The computation of the channel quality score is depicted in Equation (5). In this Equation, $(w_1, w_2, w_3, w_4, w_5, w_6, w_7)$ represents the normalized values of the various channel quality parameters, while $(\overline{PRR}, \overline{SNR}, \overline{RSSI}, \overline{r^i_{SNR}}, \overline{r^i_{RSSI}}, \overline{\sigma^2_{RSSI}}, \overline{\sigma^2_{SNR}})$ denotes the corresponding weights for each parameter. The channel quality score is derived by normalizing the sum of the products of the weights and the normalized parameters and then multiplying the result by 100.

$$score = \begin{bmatrix} w_1 & w_2 & w_3 & w_4 & w_5 & w_6 & w_7 \end{bmatrix} \begin{bmatrix} \overline{PRR} \\ \overline{SNR} \\ \overline{RSSI} \\ \overline{r^i_{SNR}} \\ \overline{r^i_{RSSI}} \\ \overline{\sigma^2_{RSSI}} \\ \overline{\sigma^2_{SNR}} \end{bmatrix} \times 100 \quad (5)$$

3.2.2. Fuzzy Analytic Hierarchy Process

The Fuzzy Analytic Hierarchy Process (FAHP) is a widely employed method in the field of decision analysis, integrating fuzzy mathematical theory with the analytic hierarchy process to address complex decision problems [24,25]. Due to the inherent imprecision of individual judgments not accounted for in the basic AHP, it has been enhanced through the incorporation of fuzzy logic methods. In FAHP, linguistic variables are utilized for pairwise comparisons of criteria and alternative solutions, represented by triangular fuzzy numbers. Within assessments, triangular fuzzy numbers can be employed to characterize the uncertainty, membership, and possibility of the impact on channel quality. This can be expressed as follows:

$$A = (x, \mu_A(x))|x \in X \quad (6)$$

Here, A represents a triangular fuzzy number, X denotes the range of values for the input variable x, and $\mu_A(x)$ signifies the membership of x, which can be expressed using a membership function:

$$\mu_A(x) = \begin{cases} \frac{x-a}{b-a}, \ a \le x \le b \\ \frac{c-x}{c-b}, \ b \le x \le c \\ 0, \ otherwise \end{cases} \quad (7)$$

In this context, $\mu_A(x) \in [0,1]$, a, b, and c, respectively, denote the values of the left, middle, and right vertices of the triangle on X. The value of b represents the highest degree of truth; it is interpreted as a more appropriate estimate, while the values of a and c reflect the expert's reservations: the wider the base of the triangle, the greater the uncertainty of the opinion. A narrower triangle indicates greater confidence in the decision made by the expert. Assuming the following fuzzy numbers $\widetilde{M}_1$ and $\widetilde{M}_2$, specified by three digits (a_1, b_1, c_1) and (a_2, b_2, c_2), the fundamental operations for triangular fuzzy numbers are described as follows:

$$\begin{aligned} &\widetilde{M}_1 \oplus \widetilde{M}_2 = (a_1, b_1, c_1) \oplus (a_2, b_2, c_2) = (a_1 + a_2, b_1 + b_2, c_1 + c_2) \\ &\widetilde{M}_1 \otimes \widetilde{M}_2 = (a_1, b_1, c_1) \otimes (a_2, b_2, c_2) = (a_1 a_2, b_1 b_2, c_1 c_2) \\ &(a_1, b_1, c_1)^{-1} = (\tfrac{1}{c_1}, \tfrac{1}{b_1}, \tfrac{1}{a_1}) \\ &\widetilde{M}1^{\widetilde{M}_2} \cong ({a_1}^{a_2}, {b_1}^{b_2}, {c_1}^{c_2}) \end{aligned} \quad (8)$$

The weights of the parameters at each level are determined using the concept of geometric mean. The geometric mean of the corresponding row parameters' crisp matrix, denoted as GM_i, can be determined using Equation (9), where b_{ij} in Equation (9) represents the values in the crisp comparison matrix for the i-th row and j-th column. Here, M denotes the number of parameters in the comparison matrix.

$$GM_i = \left[\prod_{j=1}^{M} b_{ij} \right]^{\frac{1}{M}} \quad (9)$$

The weight of the variable can be determined using Equation (10).

$$w_i = GM_i / \sum_{i=1}^{M} GM \tag{10}$$

The relative importance scale in normal AHP is 1 to 9, whereas in FAHP, it is $\overline{1}$ to $\overline{9}$. Table 1 presents the fuzzy relative importance table, where α denotes a fuzzification factor.

Table 1. Definition of fuzzy relative importance scale.

Relative Importance	Fuzzy Scale	Meaning
$\overline{1}$	(1, 1, 1)	Indicates that two factors are of equal importance.
$\overline{3}$	(3 − α), 3, (3 + α)	Suggests that the former factor is slightly more important than the latter.
$\overline{5}$	(3 − α), 5, (3 + α)	Denotes that the former factor is significantly more important than the latter.
$\overline{7}$	(3 − α), 7, (3 + α)	Highlights that the former factor is strongly more important than the latter.
$\overline{9}$	(3 − α), 9, (3 + α)	Emphasizes that the former factor is extremely more important than the latter.
$\overline{2}, \overline{4}, \overline{6}, \overline{8}$	(x − α), x, (x + α)	Intermediate values between two adjacent judgements.

3.2.3. Entropy Weight Method

The Entropy Weight Method is a multi-criteria decision analysis technique used to determine criteria weights based on information entropy. Entropy reflects the diversity and uncertainty of criteria, with higher entropy indicating a more significant disparity between criteria and lower weights. In comparison, lower entropy signifies greater consistency between criteria and higher weights. The total entropy of the criterion set can be obtained by calculating the entropy of each criterion. Subsequently, the criteria weights are determined based on their contributions to the total entropy. The Entropy Weight Method is widely applied in problems involving multiple criteria decision-making, evaluation, and ranking, as it considers the diversity and importance of criteria, providing an objective, quantitative method for weight determination.

The specific calculation steps are as follows:

Step 1: Construct a decision matrix where each column represents a criterion, and each row represents an alternative solution.

$$X = \begin{bmatrix} x_{11} & \cdots & x_{1\mathrm{n}} \\ \vdots & \ddots & \vdots \\ x_{m1} & \cdots & x_{mn} \end{bmatrix} \tag{11}$$

Step 2: Normalize the decision matrix.

$$Q_{ij} = \frac{x_{ij} - \min(x_{ij})}{\max(x_{ij}) - \min(x_{ij})} \tag{12}$$

Step 3: Calculate the entropy of each criterion, defining "entropy". When there are m evaluation factors and n evaluation objects in the evaluation index system, the entropy of the index is defined as:

$$H_i = -k\sum_{j=1}^{m} f_{ij} \ln f_{ij} \tag{13}$$

where $f_{ij} = \frac{Q_{ij}}{\sum_{j=1}^{m} Q_{ij}}$, $k = \frac{1}{\ln n}$, and when $f_{ij} = 0$, let $f_{ij} \ln f_{ij} = 0$.

Step 4: Define the entropy weight and calculate the contribution of each criterion to the total entropy by dividing the entropy of each criterion by the total entropy to obtain the weight of each criterion.

$$W_i = \frac{1 - H_i}{m - \sum_{j=1}^{m} H_i} \tag{14}$$

where $W_i \in [0,1]$, $\sum_{i=1}^{m} W_i = 1$.

3.2.4. Combining Weighting Algorithm

Diakoulaki proposed the criteria's importance through inter-criteria correlation (CRITIC) as a means to assign proportional weights objectively to different dimensions of indicators in multi-attribute problems [26]. This method objectively assigns weights based on the contrast of the same indicators for different evaluation objects and the conflict between different indicators, characterizing the importance and influence of each indicator in the evaluation process according to the assigned weight values. The specific steps are as follows.

Step 1: Consider n variables, each with n indicators, forming the original decision matrix $X = (x_{ij})_{m \times n}$. As the dimensions of each indicator are not identical, non-dimensional processing should be performed separately for positive and inverse indicators to make the decision matrix more standardized, resulting in a standardized matrix.

$$X' = (x'_{ij})_{m \times n} \tag{15}$$

Step 2: Calculate the standard deviation of j indicators for i variables to characterize the contrast of the indicators, denoted as σ_j, as shown in the following equation:

$$\sigma_j = \sqrt{\frac{1}{m-1} \sum_{i=1}^{m} \left(x'_{ij} - \frac{1}{m} \sum_{i=1}^{m} X'_{ij} \right)^2} \tag{16}$$

Step 3: Calculate the correlation r_{uj} between the u-th and j-th indicators to represent the conflict between indicators R_j, as shown in the following equation:

$$r_{uj} = \frac{\sum\limits_{u,j=1}^{n} (x_u - \overline{x}_u)(x_j - \overline{x}_j)}{\sqrt{\sum\limits_{u=1}^{n} (x_u - \overline{x}_u)^2 \sum\limits_{j=1}^{n} (x_j - \overline{x}_j)^2}} \tag{17}$$

$$R_j = \sum_{u=1}^{n} (1 - |r_{uj}|) \tag{18}$$

where $u = 1, 2, \cdots, n; j = 1, 2, \cdots, n$.

Step 4: Based on the contrast and conflict of the indicators, determine the information content latent in the n indicators, denoted as S_j, as shown in the following equation:

$$S_j = \sigma_j \cdot R_j \tag{19}$$

Step 5: Calculate the objective weight w_j, as shown in the following equation:

$$w_j = \frac{S_j}{\sum\limits_{j=1}^{n} S_j} \tag{20}$$

3.3. Foundations of Channel Quality Level Assessment Theory

The Gated Recurrent Unit (GRU) Model

The GRU [27] is a computationally efficient, structurally simple recurrent neural network classification algorithm adept at capturing long-term dependencies and exhibiting strong modeling capabilities for sequential data. It excels in learning long-term memory while maintaining a low model complexity, achieving high predictive accuracy. The schematic diagram of GRU is depicted in Figure 1, and its forward propagation formula is articulated as follows:

$$r_t = \sigma(W_r \times [h_{t-1}, x_t] + b_r) \tag{21}$$

$$z_t = \sigma(W_z \times [h_{t-1}, x_t] + b_z) \tag{22}$$

$$\widetilde{h_t} = \tanh(W_h \times [r_t \odot h_{t-1}, x_t] + b_h) \tag{23}$$

$$h_t = (1 - z_t) \odot h_{t-1} + z_t \odot \widetilde{h_t} \tag{24}$$

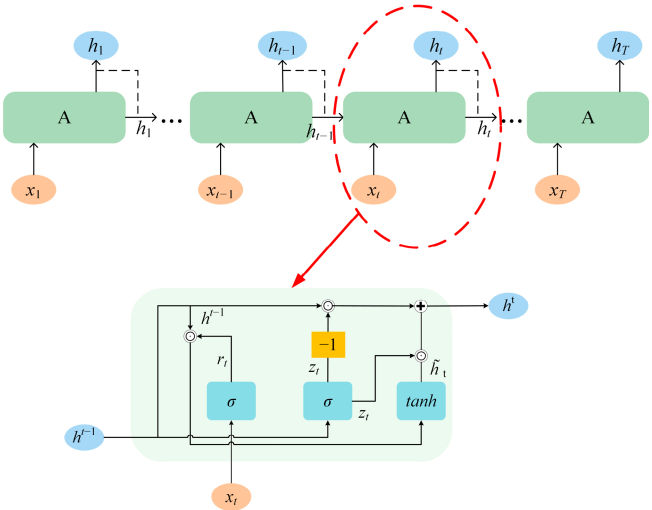

Figure 1. Schematic representation of the gated recurrent unit mechanism.

In the above equation, W and b denote the network parameters; x_t represents the sequential value at time t; h represents the hidden state at time t; σ(·) signifies the activation function; tanh(·) denotes the hyperbolic tangent function; $\odot$ represents the element-wise product operator; r_t denotes the vector controlling the resetting of the hidden state; z_t signifies the vector controlling the update of the hidden state; $\widetilde{h_t}$ represents the candidate hidden state at time t, and is a vector used for the computation of the hidden state.

3.4. The Fundamental Theory of Channel Quality Grading Evaluation

3.4.1. The VMD Algorithm

The Variational Mode Decomposition (VMD) algorithm is a fully non-recursive adaptive data processing method that determines the number of decompositions based on the inherent characteristics of the data. It then transforms the data to obtain the optimal solution, extracting practical separated components by updating central frequencies and modal functions to derive intrinsic mode functions. The VMD algorithm comprises the construction of variation and the resolution of variation [28].

The construction of variation involves decomposing the original data into several modal components, minimizing the sum of the decomposition bandwidths for each mode. This can be expressed as:

$$\min\left\{\sum_{m=1}^{m}\left\|\partial_t\left\{\left[\delta(t) + \frac{\mathrm{j}}{\pi t}\right] * u_m(t)\right\}e^{-\mathrm{j}\omega_m t}\right\|_2^2\right\}, \tag{25}$$

$$s.t.\sum_m u_m(t) = f(t) \tag{26}$$

where $\delta(t)$ represents the Dirac function; j is the imaginary unit. $f(t)$ represents the original input signal. $*$ denotes the convolution operator; m signifies the number of decomposed modes; $\{u_m\}$ indicates the m-th modal component; and $\{\omega_m\}$ illustrates the central frequency of the m-th part. By introducing a quadratic penalty factor, α, and a Lagrange multiplier operator, λ, an unconstrained variational problem can be formulated as:

$$L(\{u_m\},\{\omega_m\},\lambda) = \alpha\sum_m\left\|\partial_t\left\{\left[\delta(t) + \frac{\mathrm{j}}{\pi t}\right] * u_m(t)\right\}e^{-\mathrm{j}\omega_m t}\right\|_2^2 + \left\|f(t) - \sum\nolimits_m u_m(t)\right\|_2^2 + \left\langle \lambda(t), f(t) - \sum_m u_m(t)\right\rangle \tag{27}$$

Utilizing the alternating direction multiplier iteration algorithm facilitates the optimization of the modal components and central frequencies while seeking the saddle point of the augmented Lagrangian function. The solutions for $\hat{u}_m$, ω_m, and $\hat{\lambda}$ post-iteration can be obtained as follows:

$$\hat{u}_m^{n+1}(\omega) = \frac{\hat{f}(\omega) - \sum\limits_{i<m} \hat{u}_m^{n+1}(\omega) + \frac{\hat{\lambda}^n(\omega)}{2}}{1 + 2\alpha(\omega - \omega_m^n)^2} \tag{28}$$

$$\omega_m^{n+1} = \frac{\int_0^\infty \omega \left|\hat{u}_m^{n+1}(\omega)\right|^2 d\omega}{\int_0^\infty \left|\hat{u}_m^{n+1}(\omega)\right|^2 d\omega} \tag{29}$$

$$\hat{\lambda}^{n+1}(\omega) = \hat{\lambda}^n(\omega) + \tau(\hat{f}(\omega) - \sum_m \left|\hat{u}_m^{n+1}(\omega)\right|) \tag{30}$$

where τ serves as the noise tolerance to ensure the fidelity of the signal decomposition; $\hat{u}_m(\omega)$, $\hat{f}(\omega)$, and $\hat{\lambda}(\omega)$ represent the Fourier transforms of u_m, ω_m, and λ, respectively.

3.4.2. The BiLSTM Algorithm

The Long Short-Term Memory (LSTM) is an improvement over traditional recurrent neural networks (RNNs). Its structure addresses excessive weight impact during RNN training and gradient vanishing, exhibiting superior handling of long-time series. While a unidirectional LSTM can yield favorable results when the critical information of input features is fixed at a specific position, such as the middle or the end, it may fail to capture crucial information if it resides at the beginning or is not fixed in place. Hence, the Bi-LSTM was introduced [29]. To enable the output layer to assimilate past and future information, the input time series is fed forward and backward into two LSTM modules, with their outputs combined and transmitted to the output layer. This resolves the issue of the temporal sequence of information and simultaneously considers the changing patterns of past and future data, thereby demonstrating superior performance. The schematic of the Bi-LSTM algorithm is depicted in Figure 2.

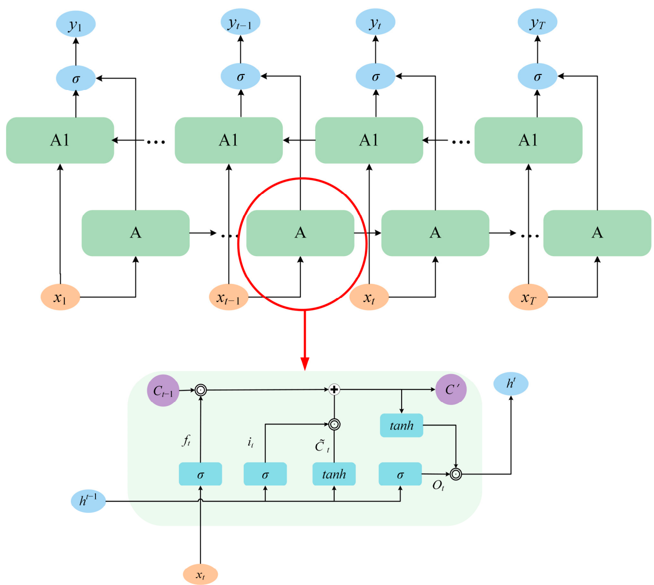

Figure 2. Schematic representation of the Bi-LSTM algorithm.

1. The Forget Gate

At the outset, the forget gate determines the information to be discarded from the current state input, utilizing an activation function to forget information selectively.

$$f_t = \sigma\left(W_f \times [h_{t-1}, x_t] + b_f\right) \tag{31}$$

Here, the symbol σ represents the sigmoid activation function, which transforms the input into the interval [0, 1], thus enabling partial input to be transformed into 0, thereby serving the process of forgetting. The hyperbolic tangent (tanh) is also an activation function, changing the information into the interval [−1, 1]. The characteristics of these two activation functions are depicted in Figure 3.

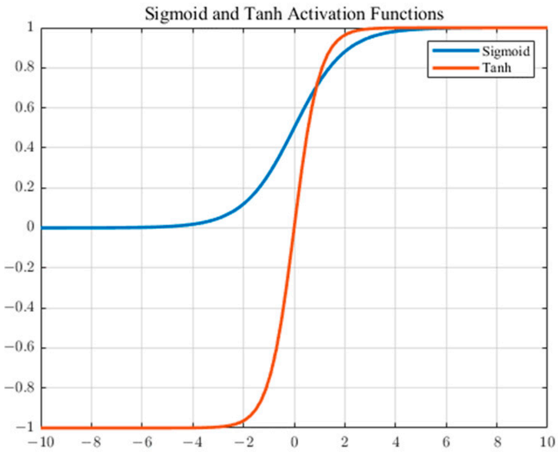

Figure 3. Activation function.

Where W_f represents the weight parameter connecting the input to the hidden layer neurons of the forget gate, with the input features being of dimension m_1 and the number of hidden layer neurons denoted as m_2. Therefore, W_f is an $(m_1 + m_2) \times m_2$ matrix. b_f signifies the bias of the forget gate's hidden layer, with the same number of neurons as the hidden layer. h_t denotes the network output at the previous time step, while x_t represents the input to the network at time step t.

2. The Input Gate

The input gate primarily determines which information is adopted for updating.

$$i_t = \sigma(W_i \times [h_{t-1}, x_t] + b_i) \tag{32}$$

$$\widetilde{C}_t = \tanh(W_C \times [h_{t-1}, x_t] + b_C) \tag{33}$$

Tanh constrains the output to the range of [−1, 1], where W_i and W_c represent the parameters connecting the input to the hidden layer neurons, and b_i and b_C represent the biases.

The new state is obtained by adding the information passed through the forget gate to the information newly introduced through the input gate.

$$C_t = C_{t-1} \odot f_t + \widetilde{C}_t \odot i_t \tag{34}$$

3. The Output Gate

Utilizing the newly formed memory, C_t, in conjunction with the proportion calculated by the final gate, yields the ultimate output. Here, W_o denotes the weight of the output gate, while b_o represents the bias of the output gate.

$$O_t = \sigma(W_o \times [h_{t-1}, x_t] + b_o) \tag{35}$$

$$h_t = O_t \odot \tanh(C_t) \tag{36}$$

4. Establishment and Validation of Channel Quality Assessment and Prediction Models

This study investigates the channel quality evaluation model in V2I scenarios, thus necessitating the consideration of the impact of different services and vehicle movements on the assessment of channel quality. In the V2I scenario, services can be categorized based on the frequency of business data reporting into fast services (sending one data packet per second), slow services (sending one data packet per minute), and very slow services (sending one data packet per hour). Furthermore, services can be classified according to their importance into general, relatively significant, and highly important services. In the V2I scenario, there are five primary types of services: obtaining weather data, obtaining road conditions, obstacle avoidance reminders, emergency evasion, and vehicle information reporting. These five services are classified based on their frequency and importance, as depicted in Table 2.

Table 2. Classification of V2X service characteristics.

Business Name	Frequency	Importance
Obstacle Avoidance	High	Extremely Important
Emergency Evacuation	High	Extremely Important
Vehicle Information Reporting	Low	Moderately Important
Obtaining Road Condition Information	Low	Important
Obtaining Weather Data	Very Low	Moderately Important

The description of channel quality in most communication systems is typically based on the classification of channel quality levels. In this paper, we delineate the classification of channel quality levels based on the minimum requirements of PRR for different frequency services and the minimum demodulated signal-to-noise ratio and signal strength required for using other parameters in LoRa communication. This paper categorizes channel quality into three classes: high channel quality, medium channel quality, and low channel quality.

4.1. Establishment of a Model for the Assessment of Channel Quality Grades

The comprehensive architecture for evaluating and predicting channel quality levels, as illustrated in Figure 4, comprises five main modules: the data acquisition module, the channel quality scoring module, the spatial channel information perception module, the channel quality classification module, and the prediction module. The data acquisition module conducts statistical recording of the RSSI, SNR, and PRR data uploaded by the vehicle's onboard terminals. It then calculates the evaluation parameters introduced in this paper using relevant formulas, deriving the channel quality evaluation parameters. The channel quality scoring module generates the quality score based on the input channel quality evaluation parameters and their respective weighted values. The spatial channel information perception module outputs spatial channel quality evaluation parameters based on the location information uploaded by the vehicles. The prediction module forecasts the channel quality score and the spatial channel quality evaluation parameters for the next time step of the onboard terminals. The channel quality classification module consists of a neural network-based classifier. It takes the denoised and calibrated channel quality scores and the spatial channel quality evaluation parameters as input for automatically extracting features and classifying the channel quality levels.

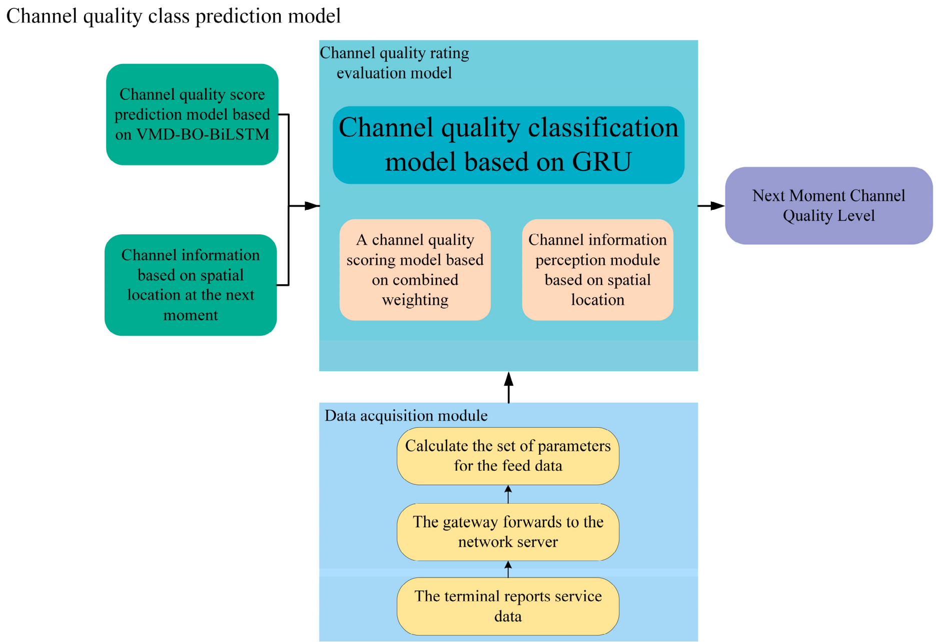

Figure 4. Overall architecture for evaluation and prediction model of channel quality grades.

4.1.1. Development of a Channel Quality Scoring Model

In this study, various aspects of network performance were considered when constructing a channel assessment model for LoRa networks in V2I scenarios. Key performance indicators were selected to propose a weight-based channel quality scoring algorithm. This algorithm combines subjective and objective combinations of seven parameters to obtain the final channel quality score. By converting the seven parameters into a single parameter through weighting, the algorithm reduces the dimensionality of input data for subsequent use of classification algorithms, thereby reducing algorithm complexity. Additionally, considering the variation in channel quality with spatial changes during vehicle motion, a transmission loss map was introduced to adjust channel quality. Ultimately, the channel quality rating model addresses the multi-classification problem of determining channel quality levels based on multiple factors.

The hierarchy of the FAHP model is designed based on different criteria and sub-criteria. All identified criteria, sub-criteria, and alternative assessment options are arranged at different levels of the hierarchy (as shown in Figure 5). The first level of the hierarchy defines the objective of the decision problem, while the second and third levels, respectively, define the criteria and parameters for measuring the quality of the communication channel.

Five experts scored the seven indicators, with higher scores indicating greater importance in the channel quality assessment model. The specific scores are illustrated in Table 3.

Table 3. Expert evaluation scores of the seven key indicators.

Category	**C1**	**C2**	**C3**	**C4**	**C5**	**C6**	**C7**
Expert 1	$\overline{5}$	$\overline{5}$	$\overline{9}$	$\overline{3}$	$\overline{5}$	$\overline{5}$	$\overline{7}$
Expert 2	$\overline{3}$	$\overline{5}$	$\overline{9}$	$\overline{5}$	$\overline{5}$	$\overline{7}$	$\overline{7}$
Expert 3	$\overline{3}$	$\overline{5}$	$\overline{7}$	$\overline{3}$	$\overline{5}$	$\overline{5}$	$\overline{5}$
Expert 4	$\overline{5}$	$\overline{5}$	$\overline{1}$	$\overline{5}$	$\overline{5}$	$\overline{5}$	$\overline{5}$
Expert 5	$\overline{3}$	$\overline{5}$	$\overline{9}$	$\overline{5}$	$\overline{7}$	$\overline{5}$	$\overline{7}$

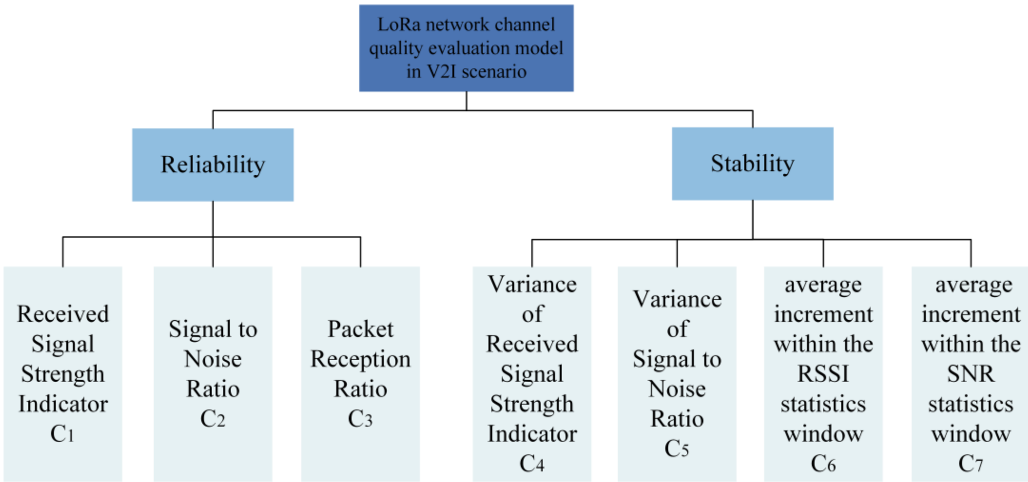

Figure 5. FAHP evaluation model for channel quality assessment.

The weights of each parameter were calculated based on the fuzzy numbers corresponding to the scores in Table 1, and a sensitivity analysis of the proposed decision model was conducted by varying the fuzzification factor. As shown in Table 4, the model output results were analyzed using six sets of fuzzification factor values (0, 0.2, 0.4, 0.6, 0.8, and 1). The results revealed that although the weights of each communication channel parameter changed with the variation in fuzzification factor, the ranking of the parameters remained unchanged [24].

Table 4. Weights of seven parameters for different fuzzification factors (α).

Category	$\alpha = 0$	$\alpha = 0.2$	$\alpha = 0.4$	$\alpha = 0.6$	$\alpha = 0.8$	$\alpha = 1$
C1	0.0275	0.0275	0.0275	0.0276	0.0276	0.0277
C2	0.0554	0.0554	0.0556	0.0559	0.0563	0.0568
C3	0.4218	0.4216	0.4211	0.4203	0.419	0.4173
C4	0.0275	0.0275	0.0275	0.0276	0.0276	0.0277
C5	0.1158	0.1158	0.1159	0.116	0.1162	0.1164
C6	0.1158	0.1158	0.1159	0.116	0.1162	0.1164
C7	0.2362	0.2363	0.2364	0.2367	0.2371	0.2376

By following the algorithmic steps outlined in Section 3.1.1, the subjective weights were computed. Subsequently, the objective weights are computed using the requirements of the entropy weight method in Section 3.1.2. Finally, the composite weights are determined through the CRITIC algorithm, yielding the ultimate weights as depicted in Table 5. Upon obtaining the weights, the channel quality score can be computed based on the seven parameters.

Table 5. Weighting results of each parameter.

Category	C1	C2	C3	C4	C5	C6	C7
FAHP	0.0277	0.0568	0.4173	0.0277	0.1164	0.1164	0.0277
Entropy Weight	0.2095	0.1215	0.1618	0.0788	0.2766	0.0724	0.0794
Combination	0.0922	0.0798	0.3266	0.0458	0.1733	0.1008	0.1814

4.1.2. A Channel Information Perception Module Based on Spatial Location

As illustrated in Figure 6, the roadside unit can simultaneously serve vehicles A and B. Compared to vehicle A, the building between vehicle B and the roadside unit renders the spatial channel information more intricate. The spatial channel information of the moving vehicles is investigated through the profile diagram between the transmitter and receiver, as depicted in Figure 7. The channel information about the moving vehicles' spatial position is based on 3D map data. Parameters such as the latitude and longitude values of the vehicle's location and the vertical height difference between the transmitter and receiver facilitate the computation of the 3D distance between the transmitter and receiver, building density, average building height, and scene type [30]. The specifics of these features are defined as follows:

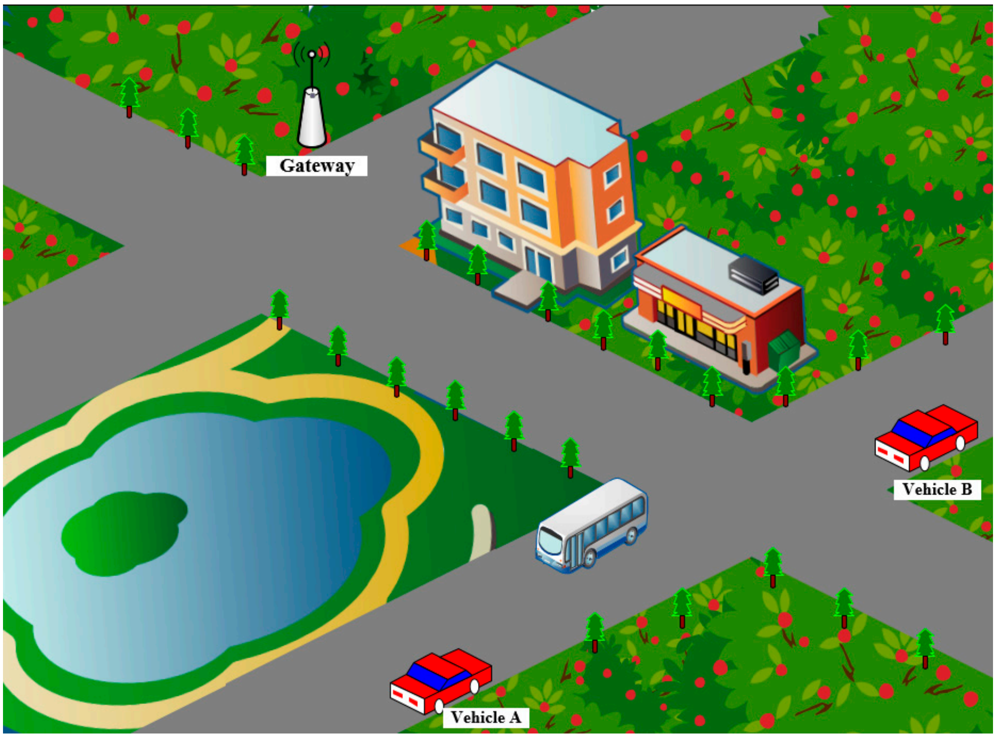

Figure 6. Deployment of V2I devices in urban settings.

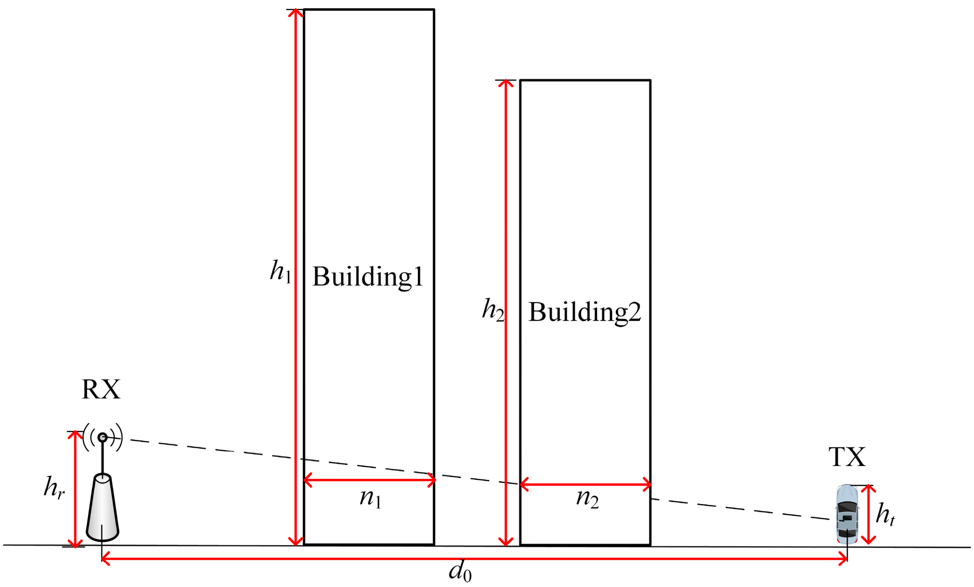

Figure 7. Depicts a cross-sectional view of the architectural composition between the RX and TX.

(1) d_{tx}, d_{ty}: Latitude and longitude of the transmitter;
(2) d_{rx}, d_{ry}: Latitude and longitude of the receiver;
(3) The 3D distance between the transmitter and the receiver, denoted as $d_z = \sqrt{(d_{tx} - d_{rx})^2 + (d_{ty} - d_{ry})^2 + (h_t - h_r)^2}$;
(4) ρ: Building density between the transmitter and receiver, calculated as the sum of the ground distances of all buildings in the profile diagram divided by the horizontal distance between TX and RX, illustrated by test point $\rho = \frac{n_1+n_2}{d_0}$ in Figure 7.
(5) h: Average building height, calculated as the total height of all buildings between TX and RX in the profile diagram divided by the number of buildings, denoted as $h = \frac{h_1+h_2}{2}$.
(6) C: Scene type, evaluated based on the 3D map information of the current location of the vehicle and the building scene between the vehicle and the roadside unit. The classic values of K can be inferred from the characteristics of the current scene.

In summary, $\{d_z, \rho, h, C\}$ constitutes the spatial channel parameters (SCP).

4.1.3. Model for Assessing Channel Quality Levels Based on GRU

The GRU model used in this study primarily consists of the GRU network introduced in Section 3.3, and the specific network model is illustrated in Figure 8. The first layer serves as the sequential input layer, followed by the GRU input layer in the second layer. The third layer, dropout, reduces data dimensionality and suppresses overfitting. Subsequently, the fourth layer is the GRU layer, followed by another dropout layer in the fifth layer to mitigate overfitting further. The sixth layer is fully connected, while the seventh layer employs the Softmax function to obtain the ultimate classification results. Finally, the last layer serves as the classification output layer.

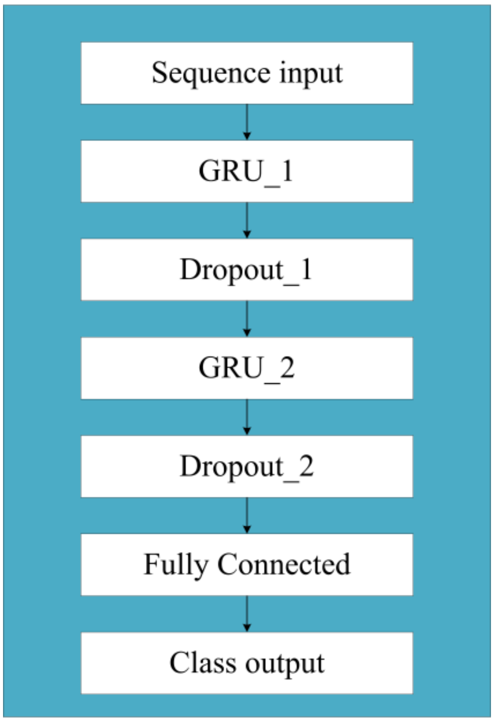

Figure 8. GRU network model.

The operational process of the model is delineated as follows:

Step 1: Data preprocessing involves implementing the 3-sigma detection method for identifying and removing outliers, employing the Z-score normalization method to transform data of varying specifications and dimensions into commensurate numerical values. The calculation formula for the Z-score is as follows [31]:

Commence by computing the mean of the original data.

$$\mu = \frac{1}{N}\sum_{i=1}^{N} x_i \tag{37}$$

Subsequently, calculate the standard deviation of the data.

$$\sigma = \sqrt{\frac{1}{N}\sum_{i=1}^{N}(x_i - \mu)}^{2} \tag{38}$$

Finally, obtain the data standardized through the Z-score method.

$$z_i = \frac{x_i - \mu}{\sigma} \tag{39}$$

Step 2: The processed sequences are input into the GRU network, wherein the gated recurrent unit extracts the temporal dependency features of interference signals, and a dropout layer is utilized to remove specific neurons from the network stochastically, thus mitigating the occurrence of overfitting.

Step 3: The extracted features are fed into the Softmax layer to yield probability values, which determine the interference signal category. Assuming there are n categories, denoted as Sk, with numerical values, the calculation formula for Softmax is as follows:

$$P(S_i) = \frac{e^{g_i}}{\sum_{k}^{n} e^{g_k}} \tag{40}$$

wherein i represents a specific category within k, and g_i signifies the value of that category.

Step 4: The classification results are generated, and the algorithm's performance is subsequently analyzed.

4.2. Construction of a Predictive Model for Channel Quality Classification

The present study has established a channel quality scoring prediction model based on VMD-BO-BiLSTM. The BiLSTM network, capable of bidirectional learning of temporal correlations between data, enhances the extraction of temporal sequence features. However, the channel quality score exhibits complex non-linear characteristics with fluctuating patterns. To address this, the VMD algorithm has been introduced to decompose the channel quality score into intrinsic mode components, thereby enabling their intuitive representation. Subsequently, different elements are incorporated into the BiLSTM model for prediction.

The Bayesian optimization algorithm, requiring only a few objective function evaluations, can obtain an optimal solution and continuously update hyperparameters [32]. This makes it suitable for addressing problems with high computational costs, unknown derivatives, and the need to determine global minima. Consequently, this study has employed the Bayesian optimization algorithm to optimize the hyperparameters of the BiLSTM model while the VMD algorithm processes the data. The VMD-BO-BiLSTM model algorithm can be categorized explicitly into data preprocessing and initialization, the Bayesian optimization phase, and the BiLSTM prediction phase, with the specific workflow of each step illustrated in Figure 9.

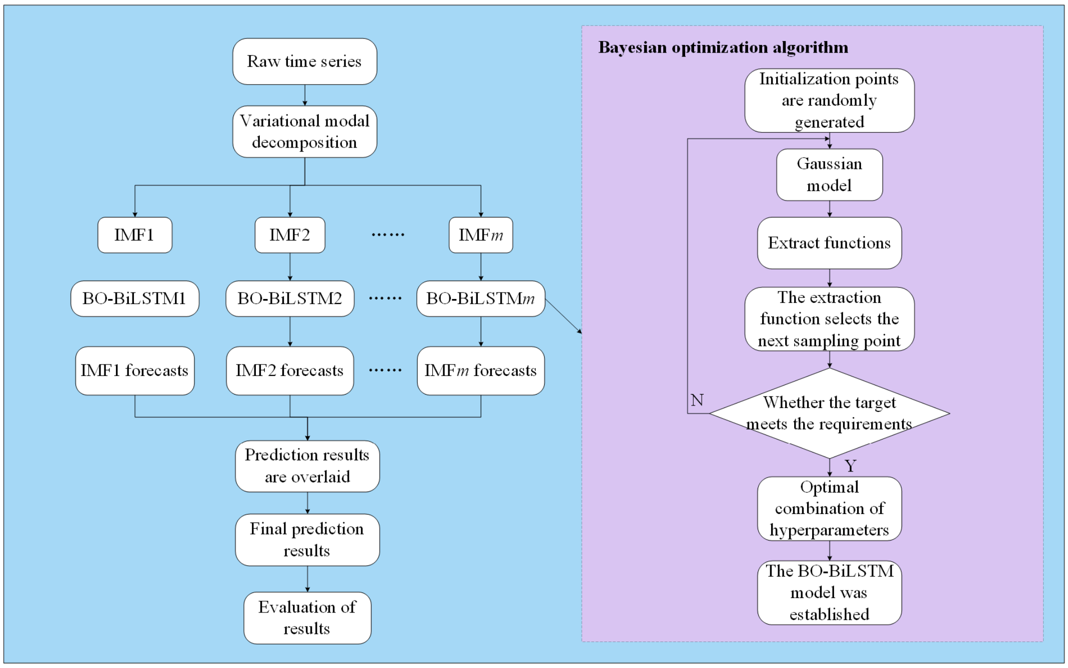

Figure 9. Outlines the procedural steps of the VMD-BO-BiLSTM algorithm.

Algorithmic Steps.

1. Data Preprocessing and Initialization

Step 1: Data Cleansing.

Initially, detection of any data gaps or anomalies is performed. In the event of missing data, linear interpolation, as presented in Equation (41), is employed for data processing. In the case of anomalous data, the use of the mean smoothing method, as indicated in Equation (42), is warranted.

$$x_{a+i} = x_a + \frac{i(x_{a+n} - x_a)}{n} \quad (41)$$

$$x_b = \frac{(x_{b+i} - x_{b-i})}{2} \quad (42)$$

Step 2: VMD Algorithm.

The dataset is partitioned into m effective modal components using the VMD algorithm, such that the sum of the decomposed bandwidths of each modal element is minimized.

Step 3: Normalization.

The data are normalized using the min-max method before training.

2. Bayesian Optimization Phase

Step 1: Initialization.

The BiLSTM model parameters and hyperparameter ranges are initialized, and random initialization points are generated. The data samples processed by the VMD algorithm and the initialized parameters are used as input variables for the Gaussian model in Bayesian optimization. Parameters are refined based on the model's predictions, aiming to improve the output results to approximate the proper distribution of the objective function.

Step 2: Evaluation.

The refined Gaussian model selects a set of parameters for evaluation. If the function achieves an optimal state closest to the objective function's proper distribution, the chosen parameter set becomes the optimal parameter set.

Step 3: Training.

The optimal parameter set is used for training in the BiLSTM. If the error of the selected parameter set is greater than the pre-set threshold, the algorithm terminates, outputting the model's predictive error and the current parameters.

Step 4: Refinement.

If the error does not meet the threshold, further refinement of the Gaussian model is carried out, returning to Step 2 until a mistake less than the pre-set threshold is achieved.

3. BiLSTM Prediction Phase

Step 1: Prediction.

The m modal components are individually input into the Bayesian-optimized BiLSTM model for prediction, and their predicted values are aggregated to obtain the overall prediction result.

Step 2: Performance Evaluation.

To assess the performance of the VMD-BO-BiLSTM model, this study employs the root mean square error (*RMSE*), mean absolute error (*MAE*), and mean fundamental percentage error (*MAPE*) as performance evaluation metrics. These are expressed by Equations (43)–(45). A decrease in *RMSE*, *MAE*, and *MAPE* indicates higher precision and reliability of the model [33].

The root mean square error is represented by:

$$RMSE = \sqrt{\frac{1}{n}\sum_{i=1}^{n}(y_i - \hat{y}_i)^2} \tag{43}$$

The mean absolute error is denoted as:

$$MAE = \frac{1}{n}\sum_{i=1}^{n}|y_i - \hat{y}_i| \tag{44}$$

The mean absolute percentage error is given by:

$$MAPE = \frac{1}{n}\sum_{i=1}^{n}\left|\frac{y_i - \hat{y}_i}{y_i}\right| \tag{45}$$

5. Experimentation and Validation

5.1. The Establishment of Testing Environments

To validate the effectiveness of the proposed channel quality level assessment and prediction methods, a vehicle equipped with a LoRa vehicular terminal was used for testing. During the testing process, packet reception rate, signal-to-noise ratio, and signal strength were collected to construct a dataset for training and analysis. The testing scenario occurred within the campus's internal roads, as shown in Figure 10, with a gateway located at point A for receiving data from the vehicular terminal. The recording points (D_enter) and (D_leave) represent the moments when the vehicle entered and exited the obstructed area of building D relative to point A, respectively. In this testing scenario, there are two main buildings, D and C. The vehicle followed a predetermined route depicted in the figure, and the vehicular terminal's data reporting was analyzed under three different link budgets of high, medium, and low by adjusting the transmission power of the vehicular terminal. The specific testing parameters are shown in Table 6 below.

Table 6. Experimental parameter table.

Parameter	Parameter Values
BW	500 KHz
Frequency	480 MHz
SF	12

Table 6. *Cont.*

Parameter	Parameter Values
Packet length	20 Bytes
CR	4/5
Preamble length	10
Transmission power	14 dBm, 17 dBm, 20 dBm
Distance	150 m
Gateway height	1 m
Data packet generation rate	1 packet/s
Vehicle speed	25 km/h

Figure 10. Deployment diagram for testing.

5.2. Validation of Model Performance

As illustrated in Figure 11, in conjunction with the time log recorded during the testing process, it is evident that the PRR noticeably decreases when the vehicle enters the obstructed area of the building. Conversely, as the vehicle exits the obstructed area, the PRR gradually increases. Furthermore, the degree of PRR variation differs with varying link budgets at the terminal, with a greater magnitude of change in PRR observed for lower link quality compared to higher link quality. This phenomenon arises because the terminal's perception of channel quality is not solely determined by the loss resulting from spatial factors between the transmitter and receiver but also correlates with the link budget during terminal operation.

Figures 12 and 13 illustrate the relationship between PRR, SNR, and RSSI variances for vehicle-mounted terminals on the same road segment under three different link budgets. From the figures, it is evident that as vehicles enter or exit regions obstructed by buildings, variations in PRR correspond to increases in both SNR and RSSI variances. Thus, the SNR and RSSI variances serve as channel stability indicators. Furthermore, the range of changes in SNR and RSSI variances differs depending on the link quality. In the case of a low-quality link budget, as shown in Figure 12a, the range of SNR variance change is 0.3–991, while the range of RSSI variance change, as depicted in Figure 13a, is 0–80.3. For a medium-quality link budget, as shown in Figure 12b, the range of SNR variance change is 3.3–408; in Figure 13b, the range of RSSI variance change is 1–33.3. Lastly, for a high-quality link budget, as illustrated in Figure 12c, the range of SNR variance change is 9.3–342, and in Figure 13c, the range of RSSI variance change is 0.2–28.3. Therefore, we can infer that the channel becomes more unstable as the link budget quality decreases. Additionally, it is worth noting that PRR values may be the same for different variance values, indicating that relying solely on PRR changes is inadequate for assessing channel stability.

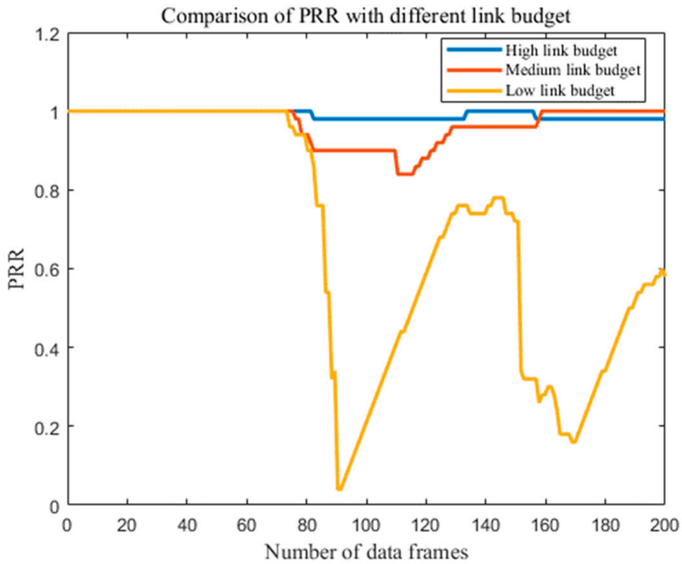

Figure 11. Comparative Graph of PRR under Varying Link Budgets.

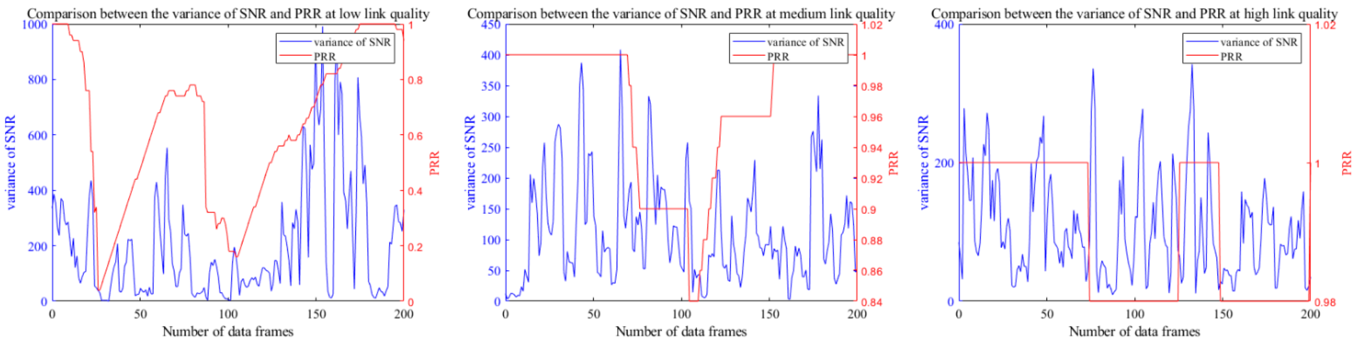

(**a**) (**b**) (**c**)

Figure 12. Comparing SNR variance and PRR under different link budgets. (**a**) Comparison of SNR variance and PRR under a high-level link budget. (**b**) Comparison of SNR variance and PRR under a medium-level link budget. (**c**) Comparison of SNR variance and PRR under a low-level link budget.

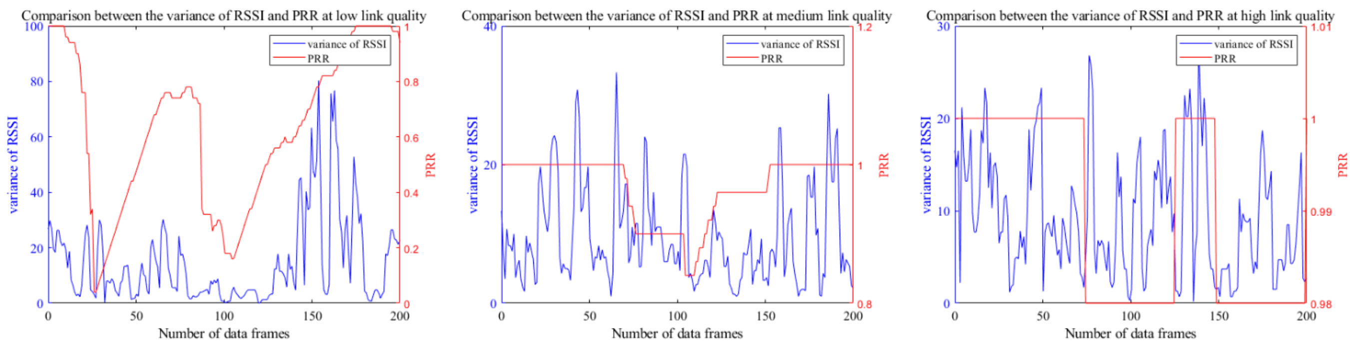

(**a**) (**b**) (**c**)

Figure 13. Comparing RSSI variance and PRR under different link budgets. (**a**) Comparison of RSSI variance and PRR under a high-level link budget. (**b**) Comparison of RSSI variance and PRR under a medium-level link budget. (**c**) Comparison of RSSI variance and PRR under a low-level link budget.

The comparative plots in Figure 14a–c depict the channel quality scores and PRR under three distinct link budget scenarios proposed in this study. It is evident that while PRR remains relatively stable, there are noticeable fluctuations in the channel quality scores. These fluctuations are correlated with the variances in SNR and RSSI. Thus, the channel quality scores proposed in this paper provide a more descriptive assessment of channel quality variability compared to PRR.

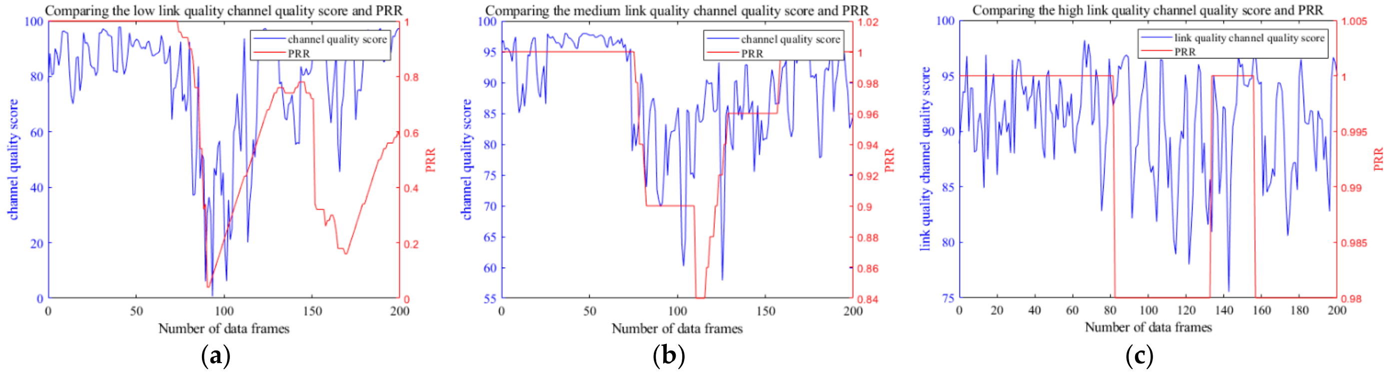

Figure 14. Comparative analysis of channel quality assessment and PRR. (**a**) A comparative plot of channel quality scores and PRR under a high-grade link budget. (**b**) A comparative plot of channel quality scores and PRR under a medium-grade link budget. (**c**) A comparative plot of channel quality scores and PRR under a low-grade link budget.

This study leverages a GRU-based model for evaluating the quality grades of channels, incorporating spatial channel information of vehicle locations and channel quality scores as input, and generating channel quality grades as output. The model is trained on a large dataset and the final results are depicted in Figure 15, showcasing a comparison between the classification outcomes and the original data. Category 1 in the figure corresponds to low channel quality, Category 2 to medium channel quality, and Category 3 to high channel quality. The accuracy achieved in the campus road scenario is 97.5%.

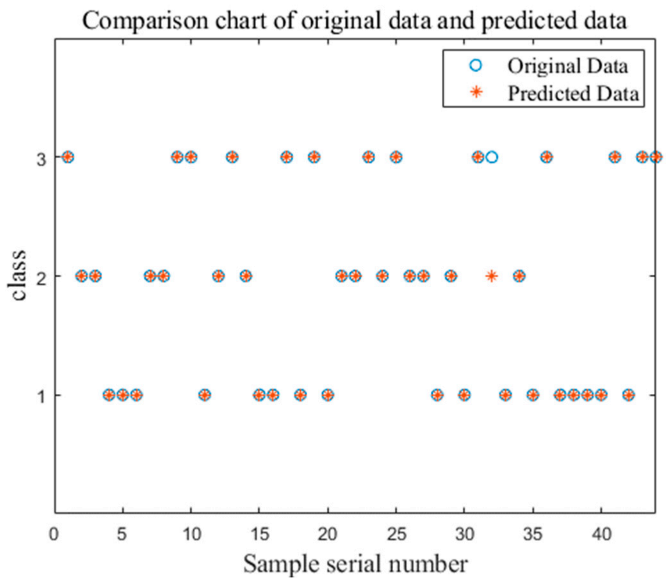

Figure 15. Presents a comparative illustration between the raw data and the results of classification.

To validate the effectiveness of the channel quality classification algorithm, the predicted data confusion matrix is shown in Figure 16a. Each column represents the expected category of the channel quality grade, while each row represents the true category. The confusion matrix shows that the proposed method accurately classifies the three-channel quality categories. Furthermore, a comprehensive evaluation of precision, recall, and F1-score for each channel quality grade is conducted by creating relevant bar charts. The accuracy, recall, and F1-score for each channel quality grade in the campus road segment scenario are depicted in Figure 16b, all within a reasonable classification range.

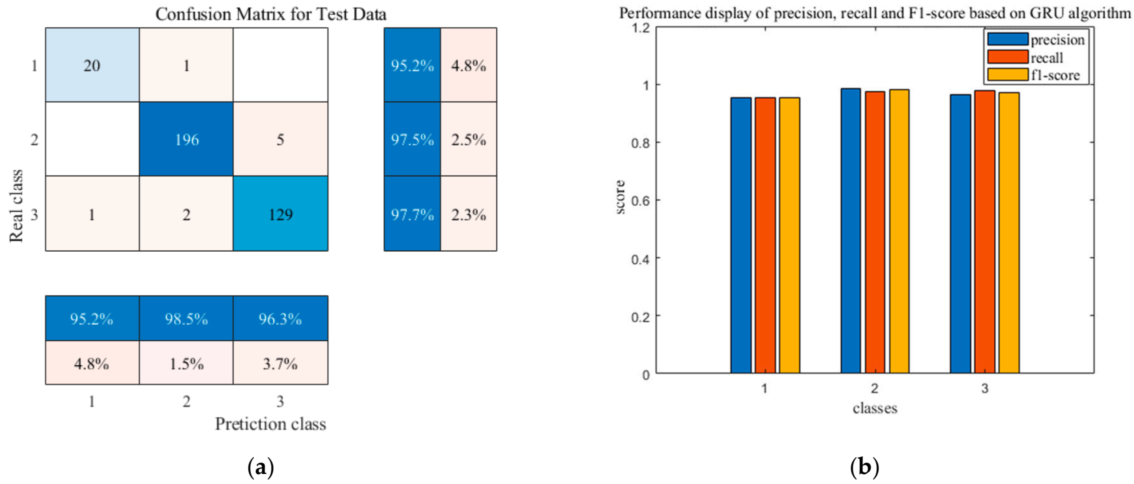

Figure 16. Performance metrics of the GRU classification algorithm. (**a**) The confusion matrix for the validation set (**b**) Accuracy, recall, and F1-score for the three different grades.

This study conducted a comparison experiment using four commonly used classification algorithms. The experimental results for different classification algorithms are shown in Table 7. The proposed GRU algorithm establishes a mapping relationship between the channel quality rating, spatial feature information of the vehicle's location, and the channel quality grade. It achieves the highest recognition accuracy when compared with four classical deep learning algorithms.

Table 7. Comparative analysis of accuracy among various classification algorithms.

Algorithm	Average Recognition Accuracy	High Channel Quality	Medium Channel Quality	Low Channel Quality	Time Overhead
SVM	88.6%	88.3%	92.3%	84.6%	0.97 s
MLP	90.1%	92.8%	92.8%	87.5%	7.69 s
CNN	93.2%	93.7%	93.7%	91.6%	52.9 s
LSTM	95.4%	93.8%	94.2%	100%	24.2 s
GRU	97.5%	97.7%	97.5%	95.2%	16.3 s

This study's proposed VMD-BO-BiLSTM prediction model takes the campus road test data samples as input and the channel ratings calculated through the channel quality rating system as output. Bayesian optimization is employed to adjust the model's hyperparameters, facilitating the identification of the optimal combination of hyperparameters and thus improving the model's performance. The VMD algorithm is further applied to decompose the original data, enhancing the accuracy of the predictions. Figure 17 illustrates the graph after VMD decomposition. To validate the algorithm's performance, a comparison is made between the performance parameters of the ordinary LSTM algorithm, the one without Bayesian optimization, the one without the VMD algorithm, and the proposed prediction model, as shown in Table 8. The table reveals that employing Bayesian optimization can reduce the algorithm's time overhead while using the VMD algorithm can enhance prediction accuracy at the cost of increased time overhead. The VMD-BO-BiLSTM algorithm used in this study achieves an R^2 value of 0.9945, demonstrating excellent performance while meeting the time constraints.

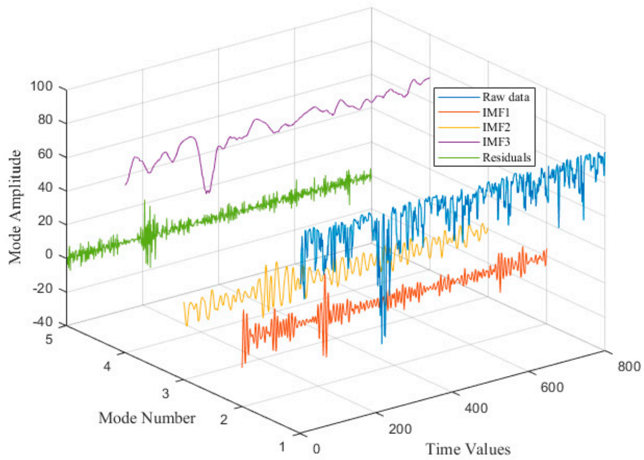

Figure 17. Showcases the decomposed outcome of the VMD algorithm for the original sequence.

Table 8. Comparative analysis of the performance of prediction algorithms.

Algorithm	MAE	MAPE	MSE	RMSE	R^2	Time Overhead
VMD-Bo-BiLSTM	0.5664	0.0129	0.58762	0.7665	0.9945	18.52 s
BiLSTM	2.1675	0.4831	7.67.4	2.7695	0.9214	13.15 s
Bo-BiLSTM	1.427	0.0333	3.0955	1.9594	0.9683	12.13 s
VMD-Bo-LSTM	0.7775	0.0180	1.1152	1.0560	0.9896	18.25 s
VMD-BiLSTM	1.8643	0.0409	5.6367	2.3742	0.9474	14.55 s

6. Conclusions

This study proposes a combined weighting-based approach to address the problem of channel quality assessment in V2I communication in mobile scenarios based on LoRa technology. This method considers the long-term and short-term variations in the channel when selecting parameters, enabling effective measurement of the continuously changing channel environment for vehicular terminals during motion. The combined weighting-based approach is also employed to calculate the channel quality rating. This evaluation method provides a more scientific description of channel quality from both subjective and objective perspectives, making it more sensitive compared to relying solely on PRR for channel quality description. In evaluating channel quality levels, the channel quality rating and spatially based channel information are utilized to characterize the channel quality levels, considering the differences in channel quality assessment for different services.

The GRU algorithm is employed to train the channel quality assessment model, achieving an accuracy of 97.5%. This research comprehensively considers the influence of space and time on channel quality levels. The prediction of channel quality levels is achieved by combining the spatial channel information of the vehicle's next moment position and predicting the corresponding channel quality score. The prediction algorithm achieves an R^2 value of 0.9945, demonstrating significantly improved accuracy compared to the unoptimized prediction algorithm. Furthermore, to ensure the generality and persuasiveness of the obtained data, the algorithm is validated in three different link quality scenarios. In this study, the vehicle's speed remains relatively stable. In future experiments, the assessment of channel quality levels during variable-speed vehicle motion will be investigated, and the proposed model will be validated using a more extensive dataset. Furthermore, the current experiments only involve single gateway data reception. The following steps will include expanding the area and increasing the number of gateways to study handover between the vehicular terminals and gateways during motion. Ultimately, the assessment of channel quality levels will be applied to network resource allocation to ensure the rationality of channel resource switching for vehicular terminals. Following the investigation of LoRa-based V2I scenarios, our team will further refine the methodology and analyze and validate the experimental data for application in 5G and V2V, extending this work to 5G and V2V scenarios.

Author Contributions: Conceptualization, S.P. and Z.L.; methodology, H.W. and Z.L.; software, Z.Y. and Z.L.; validation, W.L. and H.W.; formal analysis, S.P., R.P. and Z.L.; investigation, W.L. and R.P.; resources, R.P. and H.W.; data curation, R.P. and W.L.; writing—original draft preparation, Z.L. and Z.Y.; writing—review and editing, S.P. All authors have read and agreed to the published version of the manuscript.

Funding: This work is supported by the Key Industry Innovation Chain Project of Shaanxi Province (No. 2021ZDLGY07-10, No. 2021ZDLNY03-08), the Science and Technology Plan Project of Shaanxi Province (No. 2022GY-045),the Key Research and Development plan of Shaanxi Province (No. 2018ZDXM-GY-041), Scientific Research Program Funded by Shaanxi Provincial Education Department (Program No. 21JC030), the Science and Technology Plan Project of Xi'an (No. 22GXFW0124, No. 2019GXYD17.3), and the National Innovation and Entrepreneurship Training Program for College Students (No. 202311664021).

Data Availability Statement: Data are contained within the article.

Conflicts of Interest: The authors declare no conflicts of interest.

References

1. Wang, J.; Shao, Y.; Ge, Y.; Yu, R. A Survey of Vehicle to Everything (V2X) Testing. *Sensors* **2019**, *19*, 334. [CrossRef]
2. Toh, C.K.; Sanguesa, J.A.; Cano, J.C.; Martinez, F.J. Advances in smart roads for future smart cities. *Proc. R. Soc. A* **2020**, *476*, 20190439. [CrossRef]
3. Storck, C.R.; Duarte-Figueiredo, F. A Survey of 5G Technology Evolution, Standards, and Infrastructure Associated with Vehicle-to-Everything Communications by Internet of Vehicles. *IEEE Access* **2020**, *8*, 117593–117614. [CrossRef]
4. Xu, X.; Zeng, Z.; Wang, Y.; Ash, J.E. A Framework of a V2X Communication System for Enhancing Vehicle and Pedestrian Safety at Un-Signalized Intersections. In Proceedings of the Twelfth International Conference on Management Science and Engineering Management, Melbourne, Australia, 1–4 August 2018.
5. Available online: https://www.lora-alliance.org/ (accessed on 5 May 2022).
6. Li, Y.; Han, S.; Yang, L.; Wang, F.Y.; Zhang, H. LoRa on the Move: Performance Evaluation of LoRa in V2X Communications. In Proceedings of the 2018 IEEE Intelligent Vehicles Symposium (IV), Changshu, China, 26–30 June 2018; pp. 1107–1111.
7. Alnaeli, S.M.; Sarnowski, M.; Aman, S.; Abdelgawad, A.; Yelamarthi, K. Source Code Vulnerabilities in IoT Software Systems. *Adv. Sci. Technol. Eng. Syst. J.* **2017**, *2*, 1502–1507. [CrossRef]
8. Maitra, S.; Yelamarthi, K. Rapidly Deployable IoT Architecture with Data Security: Implementation and Experimental Evaluation. *Sensors* **2019**, *19*, 2484. [CrossRef] [PubMed]
9. Shit, R.C.; Sharma, S.; Watters, P.A.; Yelamarthi, K.; Pradhan, B.; Davison, R.; Morgan, G.; Puthal, D. Privacy-preserving cooperative localization in vehicular edge computing infrastructure. *Concurr. Comput. Pract. Exp.* **2020**, *34*, e5827. [CrossRef]
10. Ortiz, F.M.; de Almeida, T.T.; Ferreira, A.E.; Costa, L.H.M.K. Experimental vs. simulation analysis of LoRa for vehicular communications. *Comput. Commun.* **2020**, *160*, 299–310. [CrossRef]
11. Magrin, D.; Centenaro, M.; Vangelista, L. Performance evaluation of LoRa networks in a smart city scenario. In Proceedings of the 2017 IEEE International Conference on Communications (ICC), Paris, France, 21–25 May 2017; pp. 1–7.
12. Haque, K.F.; Abdelgawad, A.; Yanambaka, V.P.; Yelamarthi, K. LoRa Architecture for V2X Communication: An Experimental Evaluation with Vehicles on the Move. *Sensors* **2020**, *20*, 6876. [CrossRef] [PubMed]
13. Sun, W.; Yuan, D.; Ström, E.G.; Brannstrom, F. Cluster-Based Radio Resource Management for D2D-Supported Safety-Critical V2X Communications. *IEEE Trans. Wirel. Commun.* **2016**, *15*, 2756–2769. [CrossRef]
14. Naghsh, Z.; Valaee, S. Conflict-Free Scheduling in Cellular V2X Communications. *IEEE/ACM Trans. Netw.* **2021**, *29*, 106–119. [CrossRef]
15. Chen, C.; Liu, L.; Qiu, T.; Jiang, J.; Pei, Q.; Song, H. Routing with Traffic Awareness and Link Preference in Internet of Vehicles. *IEEE Trans. Intell. Transp. Syst.* **2022**, *23*, 200–214. [CrossRef]
16. Liu, L.; Feng, Y.; Gao, S.S.; Shu, J. Link quality estimation based on over-sampling and weighted random forest. *Comput. Sci. Inf. Syst.* **2022**, *19*, 25–45. [CrossRef]
17. Miao, W.; Ding, Z.; Tang, H.; Zeng, Z.; Zhang, M.; Zhang, S. A Seq2Seq Learning Approach for Link Quality Estimation Based on System Metrics in WSNs. *IEEE Access* **2021**, *9*, 44207–44216. [CrossRef]
18. He, M.; Shu, J. A Link Quality Estimation Method for Wireless Sensor Networks Based on Deep Forest. *IEEE Access* **2021**, *9*, 2564–2575. [CrossRef]
19. Zou, H.; Wu, Y.; Zhang, H.; Zhan, Y. Short-term Traffic Flow Prediction Based on PCC-BiLSTM. In Proceedings of the 2020 International Conference on Computer Engineering and Application (ICCEA), Guangzhou, China, 18–20 March 2020; pp. 489–493.

20. Zhang, P.; Jia, Y.; Gao, J.Z.; Song, W.; Leung, H.K.N. Short-Term Rainfall Forecasting Using Multi-Layer Perceptron. *IEEE Trans. Big Data* **2020**, *6*, 93–106. [CrossRef]
21. Kohli, P.S.; Arora, S. Application of Machine Learning in Disease Prediction. In Proceedings of the 2018 4th International Conference on Computing Communication and Automation (ICCCA), Greater Noida, India, 14–15 December 2018; pp. 1–4.
22. Wu, Z.; Pan, S.; Chen, F.; Long, G.; Zhang, C.; Yu, P.S. A Comprehensive Survey on Graph Neural Networks. *IEEE Trans. Neural Netw. Learn. Syst.* **2019**, *32*, 4–24. [CrossRef]
23. Liang, F.; Yu, W.; Liu, X.; Griffith, D.W.; Golmie, N. Toward Edge-Based Deep Learning in Industrial Internet of Things. *IEEE Internet Things J.* **2020**, *7*, 4329–4341. [CrossRef]
24. Balusa, B.C.; Gorai, A.K. Sensitivity analysis of fuzzy-analytic hierarchical process (FAHP) decision-making model in selection of underground metal mining method. *J. Sustain. Min.* **2019**, *18*, 8–17. [CrossRef]
25. Simjanovíc, D.J.; Vesíc, N.O.; Ignjatovíc, J.M.; Ranelovíc, B.M. A novel surface fuzzy analytic hierarchy process. *Filomat* **2023**, *37*, 3357–3370.
26. Diakoulaki, D.; Mavrotas, G.; Papayannakis, L. Determining objective weights in multiple criteria problems: The critic method. *Comput. Oper. Res.* **1995**, *22*, 763–770. [CrossRef]
27. Chung, J.; Gulcehre, C.; Cho, K.; Bengio, Y. Empirical Evaluation of Gated Recurrent Neural Networks on Sequence Modeling. *arXiv* **2014**, arXiv:1412.3555.
28. Liu, H.; Mi, X.; Li, Y. Smart multi-step deep learning model for wind speed forecasting based on variational mode decomposition, singular spectrum analysis, LSTM network and ELM. *Energy Convers. Manag.* **2018**, *159*, 54–64. [CrossRef]
29. Shahid, F.; Zameer, A.; Muneeb, M. Predictions for COVID-19 with deep learning models of LSTM, GRU and Bi-LSTM. *Chaos Solitons Fractals* **2020**, *140*, 110212. [CrossRef] [PubMed]
30. Cheng, H.; Ma, S.; Lee, H. CNN-Based mmWave Path Loss Modeling for Fixed Wireless Access in Suburban Scenarios. *IEEE Antennas Wirel. Propag. Lett.* **2020**, *19*, 1694–1698. [CrossRef]
31. Jane, V.A. Survey on IoT Data Preprocessing. *Turk. J. Comput. Math. Educ.* **2021**, *12*, 238–244.
32. Garnett, R. *Bayesian Optimization*; Cambridge University Press: Cambridge, UK, 2023.
33. Chicco, D.; Warrens, M.J.; Jurman, G. The coefficient of determination R-squared is more informative than SMAPE, MAE, MAPE, MSE and RMSE in regression analysis evaluation. *PeerJ Comput. Sci.* **2021**, *7*, e623. [CrossRef]